Proceedings of ASME Turbo Expo 2011
GT2011
June 6-10, 2011, Vancouver, British Columbia, Canada

GT2011-46149

EXPERIMENTAL STUDIES OF BIFURCATIONS LEADING TO CHAOS IN A LABORATORY SCALE THERMOACOUSTIC SYSTEM

Lipika Kabiraj*, **R. I. Sujith**
Department of Aerospace Engineering
Indian Institute of Technology Madras
Chennai-600036, India
lipikakabiraj@gmail.com, sujith@iitm.ac.in

Pankaj Wahi
Department of Mechanical Engineering
Indian Institute of Technology Kanpur
Kanpur-208016, India
wahi@iitk.ac.in

ABSTRACT

Bifurcation analysis is conducted on experimental data obtained from a simple setup comprising of ducted, laminar premixed conical flames to investigate the features of nonlinear thermoacoustic oscillations. It is observed that as the bifurcation parameter is varied, the system undergoes series of bifurcations leading to characteristically different nonlinear oscillations. Through the application of nonlinear time series analysis on pressure and flame (CH chemiluminescence) intensity time traces, these oscillations are characterised as periodic, aperiodic or chaotic oscillations and subsequently the nature of the obtained bifurcations is explained based on dynamical systems theory. Nonlinear interaction between the flames and the acoustic modes of the duct is clearly reflected in the high speed flame images acquired simultaneously with pressure and flame intensity measurements.*

INTRODUCTION

Practical combustion applications such as gas turbines and industrial furnaces often suffer from the problem of thermoacoustic instabilities. The instability is manifested in the form of large amplitude oscillations in pressure and heat release rate. Such oscillations can induce mechanical vibrations and increase thermal loading within the structure of the combustor. Such instabilities are more prominent in systems running on lean premixed combustion and hence, are a hindrance to the development of cleaner combustion technologies [1].

Thermoacoustic instability in combustion systems ensues as a result of a positive feedback loop between combustion and the acoustic field in the combustor. For such coupling to occur, the time scales associated with the combustion processes and the time scales associated with one or more of the acoustic modes of the combustion chamber are of the same order of magnitude [2]. Quite often, hydrodynamic phenomena, such as vortex shedding, also play an important role in the development of the instability in industrial combustors [3]. Hence, depending on the configuration of the system, several sources such as equivalence ratio fluctuations [2], vortex-flame interaction [4] and oscillatory flame area variation [5], can contribute to thermoacoustic instability. Predicting and controlling combustion instability is always a challenge because decoupling all the process responsible for the occurrence of instability restricts the modelling work and measurements in experiments [6].

Thermoacoustic oscillations are most often reported to occur in the form of limit cycles, characterized by a single dominant frequency of oscillations [2, 7, 8]. However, since several processes simultaneously contribute to the nonlinear interaction between combustion and acoustics, it is reasonable to expect a diverse nonlinear behavior of oscillations. In several numerical and experimental investigations on thermoacoustic instability, oscillations different from limit cycle oscillations have been reported. For instance, Jahnke and Culick [9] observed quasi-periodic oscillations in their continuation analysis of a uniform cross section combustor model with six longitudinal acoustic modes. Sterling [10] reported quasi-periodic oscillations in experiments on a premixed laboratory combustor, which he explains is a result

*Address all correspondence to this author of interaction between two acoustic modes of the combustor. He also observed transition of limit cycle oscillations to chaotic oscillations through bifurcation analysis of simple models incorporating nonlinear combustion. Chaotic oscillations were observed by Lei and Turan [11] in the bifurcation analysis of a simplified one-mode thermoacoustic model employing simple harmonic oscillatory heat release rate.

Here, we focus on studying the characteristics of the thermoacoustic oscillations through an experimental bifurcation analysis. Variation of the control parameter in our thermoacoustic system results in several bifurcations and a variety of complex oscillations - periodic, quasi-periodic, frequency-locked and chaotic. The location of the flames with respect to the enclosing duct is chosen as the control parameter in the bifurcation analysis. As the flame location is varied, self excited oscillations emerge in the system due to coupling between heat release rate from the flames and acoustic modes of the duct. The oscillations are recorded in terms of pressure oscillations in the duct, flame intensity fluctuations due to flame surface area modulations and high speed flame images. Subsequently, we characterize the resulting complex oscillations through reconstructed phase portraits from the acquired time series data. The observations reported in this paper shed light on the interesting nonlinear dynamics exhibited by thermoacoustic systems.

EXPERIMENTAL SETUP

The bifurcation analysis is conducted on a premixed combustor, as depicted in Fig. 1. A multipoint injection , one similar to the configuration used in investigations by Matsui [12], and recently by Noiray *et al.* [13], is used for the burner. In the current setup, there are seven conical LPG (Liquefied Petroleum Gas)-air premixed flames (A) anchored on a 18 *mm* thick copper block. The top view of the burner is given on the top right of Fig. 1. In preliminary experiments, it was observed that the onset of instability causes flame blowout. In order to facilitate investigations, a fine wire mesh is used to stabilize the flames. The burner tube (C) is 800 *mm* long with an inner diameter of 14 *mm* and thickness of 1.5 *mm*. The burner is connected to a decoupler (D) as shown, which is in turn connected to a premixing chamber (E) for enhanced mixing of the fuel and the air. The burner tube is enclosed in a glass duct (B), 800 *mm* long, closed at the bottom. This glass duct acts as the combustion chamber. During the experiments, the acoustic modes of the duct get coupled with the heat release rate fluctuations leading to self-excited oscillations. For the results on bifurcation analysis reported in this paper, the equivalence ratio, ϕ, is kept constant at 0.50 by keeping the volumetric fuel flow rate ($\mathscr{V}_f$) at 68 *ccm* and the volumetric air flow rate ($\mathscr{V}_a$) at 4000 *ccm*, measured using rotameters with an accuracy of 2%. The corresponding uncertainty in the equivalence ratio is estimated to be 2.8%. Three pressure microphones (model no. 103B02, PCB piezotronics make), P1, P2 and P3, mounted on the walls of the glass duct, as shown in Fig. 1, were installed to monitor the unsteady pressure oscillations. The results reported in this paper are based on pressure time series ($p(t)$) obtained from the microphone P1, which is mounted at a distance of 20 *cm* from the top. A 16-bit analog to digital conversion card (NI-6143) was used for data acquisition which has a resolution of 0.15 *mV* taking the input voltage range as $\pm 5V$. The uncertainty in pressure microphone measurement is 0.14 *Pa*. The intensity fluctuations ($I(t)$), proportional to the heat release rate oscillations in the flame, were detected simultaneously with pressure oscillations using a photomultiplier tube (model no. H5784, Hamamatsu make) equipped with a CH* filter (bandwidth 10 *nm*, centered at 431.4 *nm*). High speed flame images, were recorded simultaneously at a recording speed of 5000 frames per second , using a Phantom v12.1 high speed camera. The flame location was measured using a ruler with a least count of 1 *mm*.

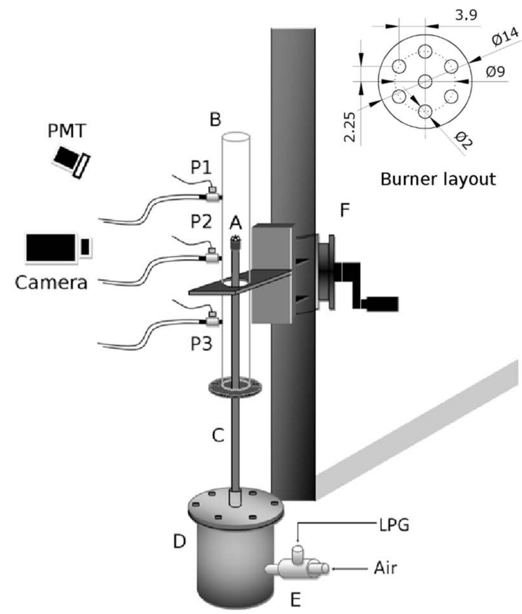

FIGURE 1: SCHEMATIC OF THE THERMOACOUSTIC SETUP, A- PREMIXED MULTIPLE FLAMES, B- OPEN-CLOSED GLASS DUCT, C- BURNER TUBE, D- DECOUPLER, E- LPG-AIR PREMIXER, F-TRAVERSE, P1, P2, P3-PRESSURE SENSORS. A TOP VIEW OF THE BURNER IS GIVEN AT THE TOP RIGHT CORNER OF THE FIGURE. ALL DIMENSIONS ARE IN *MM*.

RESULTS

Figure 2 shows the stability diagram of the system for an air flow rate of $\mathscr{V}_a$= 4000 *ccm*. For the diagram, the stability of the system at each fuel flow rate $\mathscr{V}_f$, with variation in the flame

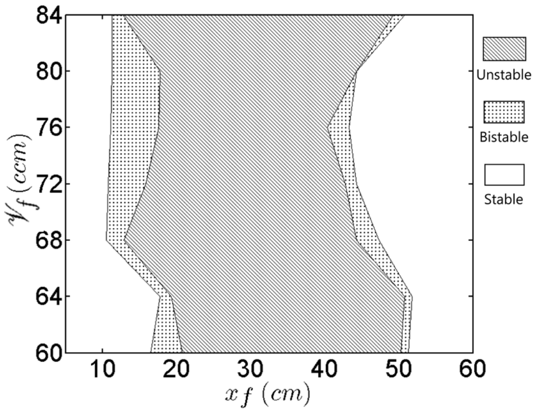

FIGURE 2: STABILITY MAP OF THE SYSTEM INDICATING THE STABILITY REGIMES OF THE SYSTEM FOR A AIR FLOW RATE (4000 *CCM*).

location is plotted. The dark shaded region of the plot represents the conditions for which the system is unconditionally unstable. The dotted region, is stable/unstable depending on whether these regions are approached from a stable/unstable condition. This region is known as the bistable region. The non-shaded regions in the stability diagram indicate stability. Although, the stability diagram successfully indicates the set of parameter values (here, the flame location and the fuel-flow rate) for which the system is stable/unstable, but it is inadequate to explore the dependence of the nonlinear characteristics of thermoacoustic instability on different parameters. For this purpose, we present the bifurcation analysis of the system. The flame location has been chosen as the control parameter for bifurcation studies. The advantage of choosing flame location over other parameters is that the system response to any variation will be immediate. In addition, flame location could be conveniently and precisely controlled for the setup and we can have a large range of control parameter values to explore the bifurcations. We will now examine at the changes in the behavior of the system with respect to changes in flame location for a constant equivalence ratio (ϕ) of 0.50 by keeping the fuel flow rate ($\mathscr{V}_f$) constant at 68 *ccm* and the air flow rate ($\mathscr{V}_a$) at 4000 *ccm*.

Bifurcation analysis

A qualitative change in the behavior exhibited by any dynamical system on varying a control parameter is termed as bifurcation. Bifurcation plot for the system under investigation is given in Fig. 3. The horizontal axis represents the flame location relative to the duct, measured from the open end of the duct (see Fig. 1). The total length of the glass duct, as mentioned already, is 80 *cm*. The bifurcation plot (Fig. 3) has been shown till flame location $x_f = 50$ *cm* as the system remains stable (fixed point) beyond this point. The vertical axis is the pressure amplitude

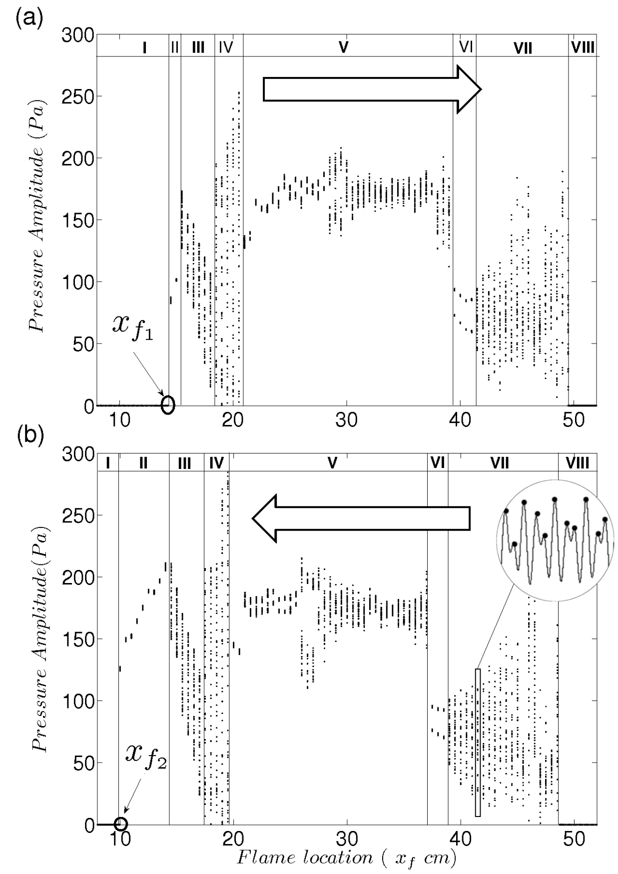

FIGURE 3: BIFURCATION DIAGRAM WITH RESPECT TO FLAME LOCATION ($\mathscr{V}_a = 4000$ *CCM*, $\mathscr{V}_f = 68$ *CCM*). THE BLOCK ARROWS INDICATE THE DIRECTION OF CHANGE IN THE FLAME LOCATION. (a) INCREASING FLAME LOCATION AND (b) DECREASING FLAME LOCATION. LOCAL MAXIMA IN THE PRESSURE TIME SERIES HAVE BEEN PLOTTED FOR EACH FLAME LOCATION. INSET SHOWS A FEW CYCLES OF A SAMPLE TIME SERIES WITH LOCAL MAXIMA MARKED WITH BLACK DOTS.

in *Pascals* obtained from pressure microphone *P*1 (Fig. 1). For each flame location, local maxima from the corresponding pressure time series, about 100 cycles long, have been plotted. For a limit cycle oscillation, this will be a single point, corresponding to the peak amplitude of the oscillation. Figure 3(a) represents the bifurcation diagram for increasing flame location and Fig. 3(b) for decreasing flame location. While increasing the flame location, the system jumps from a stable to an unstable state at $x_f = 13.5$ *cm* (x_{f_1}). The set of y ordinates corresponding to this particular x_f is a single point, indicating that the amplitudes of all the local maxima in the pressure time series are of the same magnitude and hence, the oscillations present at the particular location are limit cycle oscillations. As we go beyond this point, limit cycle oscillations exist till $x_f = 14$ *cm*. At this point, there is sudden change in the behavior of oscillations - a second bifurcation occurs. The local maxima in the oscillations no longer have the constant amplitude, which as we will see later, is also reflected in the Fourier spectrum in the form of the emergence of additional frequencies. Further changing the flame location leads to a series of bifurcations in the system. The system returns to its steady state at the flame location $x_f = 48.5$ *cm*. In the reverse direction, we find that the system exhibits hysteresis for each region as shown in Fig. 3(b). This hysteresis in system behavior is evident from the fact that there is a jump from the limit cycle oscillation back to the steady state, at $x_{f_2} = 10$ *cm*, instead of x_{f_1} (Fig. 3). The hysteresis behavior suggests that the bifurcation at the onset of instability is a subcritical Hopf bifurcation. The region of hysteresis, $x_{f_1} - x_{f_2}$, is formally known as the subcritical zone or the bistable region.

From Fig. 3, it is seen that the oscillations observed in the system assume several characteristically different periodic and aperiodic states. In the following sections, the oscillating behavior obtained for each flame location (x_f) is characterized from the time series data of pressure and intensity oscillations, with the application of concepts from dynamical systems theory - phase space representation of the system and Poincaré sections. These concepts are briefly discussed below.

The state space [14–16] (or equivalently called the phase space here) is an 'N'- dimensional space, where, 'N'is the number of independent variables, also referred to as the state variables, that determine the dynamics of a system. It is a graphical approach to visualize the dynamics of systems, particularly, nonlinear systems. Coordinates corresponding to each point in the phase space completely and uniquely define the state of the system in terms of its state variables, at a particular instant of time. The phase space hence, contains all the possible states of a dynamical system under consideration. It is easily inferred that, the dimensionality of the phase space is a measure of complexity in the system dynamics. Dynamical systems with three or lesser degrees of freedom can easily be visualised in the phase space. For system with a higher degree of freedom, the projections to a two or three dimensional phase space can be visualised. If the set of equations governing the evolution of the dynamical system are at our disposal, the evolution of the state variables can be determined and therefore, the phase space can be constructed directly.

In the absence of exact governing equations, a dynamical system can still be represented in a phase space through indirect methods. It is clear from the above discussion on phase space representation that the dynamics of a system is projected onto its state variables. The system dynamics can be represented in a phase space reconstructed from scalar observations obtained in experiments [17]. The technique of phase space reconstruction has been successfully applied to experimentally obtained data for several nonlinear processes. Even in the reconstructed phase space, important properties such as the correlation dimension and the positive Lyapunov exponents are conserved and can be extracted [14].

According to Takens' embedding theorem [17] the phase space can be reconstructed using time-delayed vectors obtained from experimentally obtained time series data. For an appropriate reconstruction, two critical values have to be determined - the time delay and the embedding dimension. The time-delay should be large enough to capture true dynamics of the system, but not so large that the relation between time-delayed vectors becomes completely random. A correct embedding dimension is required to unfold the geometric structure of the actual phase space of the system in a space created by time-delayed vectors unambiguously. A three dimensional phase space representation of a dynamical system, for example, can be constructed by the vectors $s(t)$, $s(t+\tau)$ and $s(t+2\tau)$, where, $s(t)$ is the acquired time series and τ is the optimum time delay for appropriate phase space reconstruction determined from the time series itself. Again, different approaches to finding the optimal time-delay exist [18]. The first zero-crossing of the auto-correlation function and the first minima in the average mutual information curve are two of the most frequently used approaches. Since, the auto-correlation function is essentially a linear concept, the average mutual information is preferred for the analysis of nonlinear systems and has been used for the analysis of all the cases presented in this paper. The second important detail to be considered while reconstructing the phase space is the dimension chosen for reconstruction of the phase space. One could loose essential quantitative information about a system by representing it on a phase space with a dimension lower than the actual dimension. The appropriate dimension for phase space reconstruction can also be determined from the time series [19]. Several methods exist to find out the appropriate embedding dimension. In this paper, we have used the false nearest neighbor method [18].

We will now continue with the results obtained by nonlinear time series analysis of data acquired for the thermoacoustic system under study. For the results presented here, the maximum embedding dimension was found to be four. A three dimensional space was found adequate to represent the phase portrait and to identify qualitative differences between various classes of oscillations obtained. The phase space representation will be in a three dimensional space constructed from time-delayed vectors $(p(t),\ p(t+\tau),\ p(t+2\tau))$ and $(I(t),\ I(t+\tau),\ I(t+2\tau))$ obtained from pressure time series and intensity time series respectively with time delay calculated for each case. We will discuss these different regimes with reference to Fig. 3a.

Limit cycle oscillations: Region II. The appearance of periodic oscillations from a steady state is first observed in the system at $x_f = 13.5$ *cm* (see Fig. 3a). The self-excited state is a limit cycle oscillation, resulting from a Hopf bifurcation. Ow-

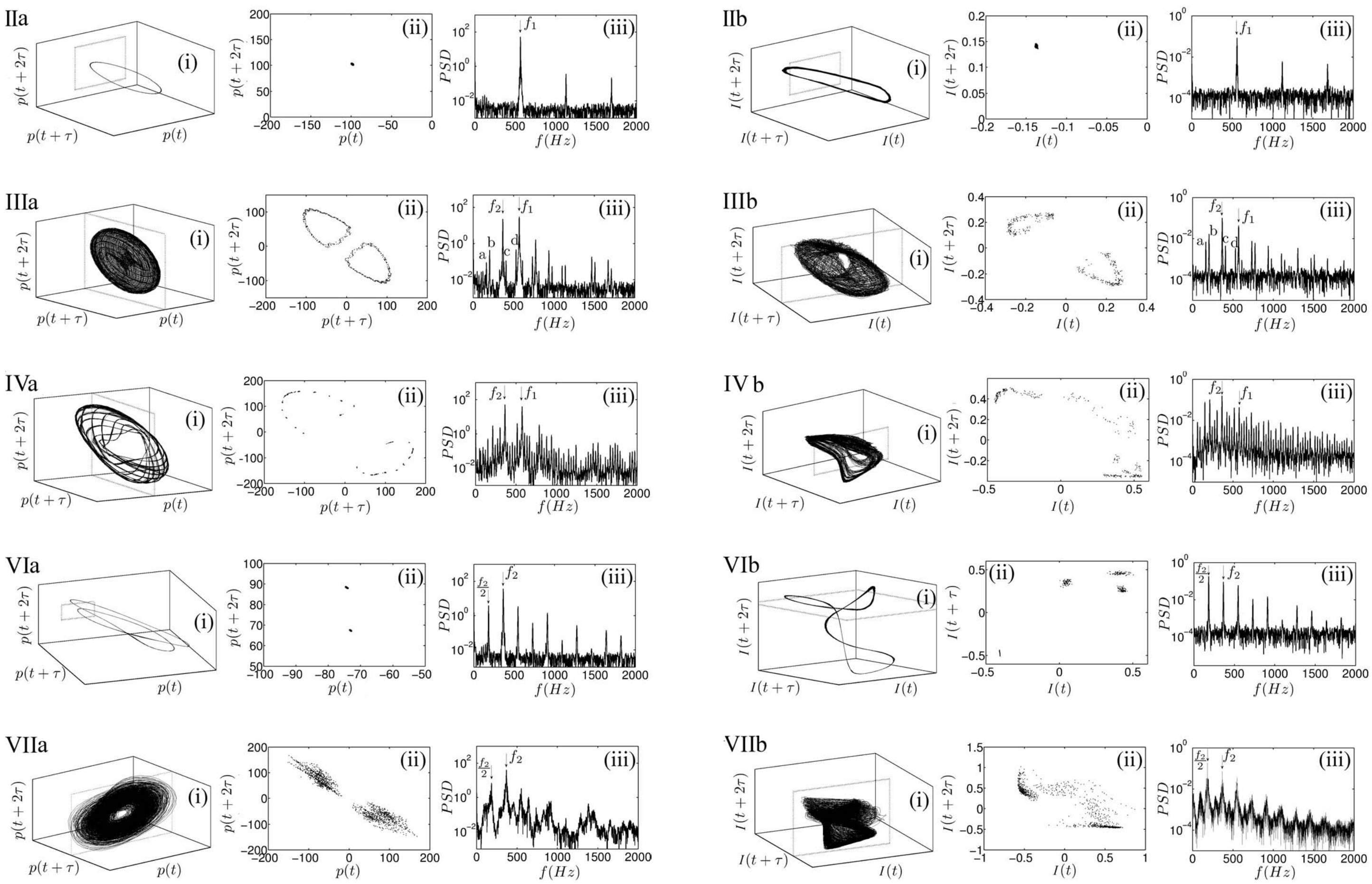

FIGURE 4: PHASE PORTRAITS (i), POINCARÉ SECTIONS (ii) AND FREQUENCY SPECTRA (iii) FOR PRESSURE TIME SERIES (LEFT HALF - a) AND INTENSITY TIME SERIES (RIGHT HALF - b), FOR DIFFERENT TYPES OF OSCILLATIONS, SEQUENTIALLY ARRANGED IN THE ORDER OF THEIR OCCURRENCE IN THE BIFURCATION DIAGRAM, FIG. 3a. $f_1 = 570.2\ HZ$, $f_2 = 366.3\ HZ$. IN FIG. IIa(iii) AND FIG. IIb(iii), MARKERS a, b, c AND d POINT TO FREQUENCIES 163.6 HZ, 202.7 HZ, 406.6 HZ AND 529.9 HZ RESPECTIVELY.

ing to the subcritical nature of the bifurcation, the change in the system dynamics is marked by an abrupt jump in the oscillation amplitude. The characteristics of the resulting oscillations are given in Figs. 4-IIa & -IIb for the pressure time series and the intensity time series respectively. The frequency spectra (Figs. 4-IIa(iii) & -IIb(iii)) shows the presence of a single frequency f_1 along with the super-harmonics. Correspondingly, structure representative of the system dynamics (referred to as the attractor henceforth) is a distinct single loop (Figs. 4-IIa(i) & -IIb(i)). To investigate the structure of the attractor, we use Poincaré sections. A Poincaré section [14] is a surface (a Poincaré plane here) in the phase space, intersecting the trajectories of the phase space attractor. In the case of a limit cycle, the intersection will give a single point, as observed in the Figs. 4-IIa(ii) & IIb(ii). The Poincaré plane for different cases represented here was chosen differently for different cases for easier visualisation of the dynamics. The Poincaré plane used for the phase portraits for limit cycle and other subsequent cases is given in the phase space diagram as a dotted rectangle.

Simultaneously acquired instantaneous flame images have been presented as images $a-h$ in Fig. 5. During the limit cycle oscillations, flames undergo sinusoidal modulations as seen from in the intensity fluctuation time series. The first six frames $a-f$ represent flame shape during different phases of oscillation, arranged in a sequence. Frames g and h are given to illustrate that for the case of limit cycle oscillations, the flame shapes occurring

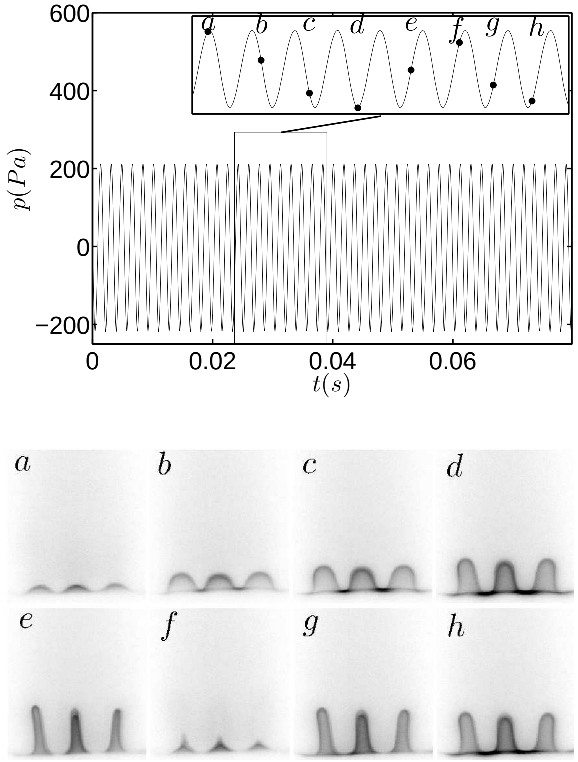

FIGURE 5: INSTANTANEOUS FLAME IMAGES FOR LIMIT CYCLE OSCILLATIONS. THE TAGGED DOTS IN THE PRESSURE TIME SERIES HAVE CORRESPONDING FLAME IMAGES MARKED BY THE SAME LOWERCASE ALPHABETS AS USED FOR THE TAGS.

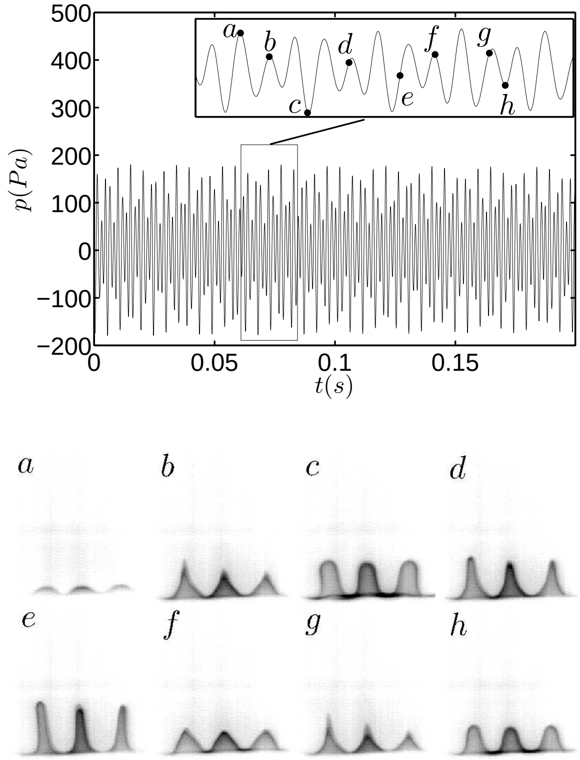

FIGURE 6: INSTANTANEOUS FLAME IMAGES FOR QUASI-PERIODIC OSCILLATIONS. THE TAGGED DOTS IN THE PRESSURE TIME SERIES HAVE CORRESPONDING FLAME IMAGES MARKED BY THE SAME LOWERCASE ALPHABETS AS USED FOR THE TAGS.

after time intervals of integral multiples of the oscillation time period are identical - as seen in image pairs *e* & *g* and *d* & *h*. This regular behavior is as expected since, the time traces also show regular behavior. As the flame location is varied further, we observe interesting changes in the dynamics of the self-excited oscillations.

Quasi-periodic oscillations: Region III. In region-III, oscillations qualitatively different from limit cycle oscillations are observed as a result of bifurcation of limit cycle oscillations. A second periodicity ensues in the system, which is revealed in the power spectrum (Figs. 4-IIIa(iii) & -IIIb(iii)) as a second frequency f_2 along with other frequencies with smaller contributions. When at least two frequencies of an oscillation are irrationally related, the oscillation will be aperiodic and the trajectories cannot form a closed loop, but instead, they evolve on the surface of a torus - a 2-torus if two such frequencies are present and covers the torus densely as it evolves. This is seen in the phase portrait in Figs. 4-IIIa(i) & -IIIb(i). Such oscillations are referred to as quasi-periodic oscillations. The Poincaré section (Figs. 4-IIIa(ii) & -IIIb(ii)), further illustrates the inner structure of the quasi-periodic attractor that we have obtained in our case. The intensity time series and the pressure time series both exhibit similar behavior in the phase space and in the power spectra. This secondary bifurcation of a limit cycle leading to the emergence of a second frequency is known formally in the theory of nonlinear dynamics as Hopf-Hopf or a Neimark-Sacker bifurcation [14].

Since, reporting a large number of flame images will not be possible, we have limited the number of image frames to eight. The differences between flame oscillation trends have been reported instead. The absence of periodicity, which was present in the case of limit cycle oscillations can also be seen in the flame shape modulations (Fig. 6). Here, although images a, b, d, f and g correspond to local maxima in the pressure time series, each of them is significantly different from the other. Images *c* and *h* are observed for two local pressure minima. The image *e*, showing an elongated flame shape, is acquired while pressure around the flame location is building up towards a local maxima.

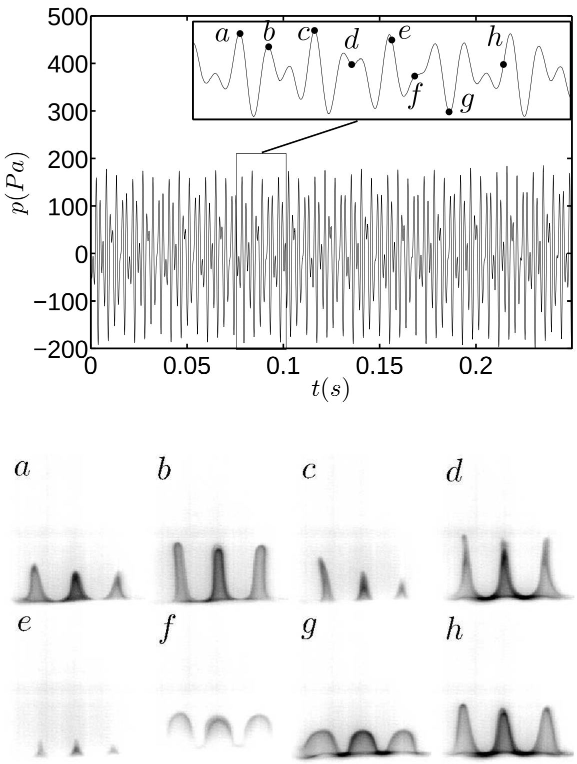

FIGURE 7: INSTANTANEOUS FLAME IMAGES FOR FREQUENCY-LOCKED OSCILLATIONS. THE TAGGED DOTS IN THE PRESSURE TIME SERIES HAVE CORRESPONDING FLAME IMAGES MARKED BY THE SAME LOWERCASE ALPHABETS AS USED FOR THE TAGS.

Frequency-locked oscillations: Region IV. As the trajectories are moving on the surface of the torus, the frequencies become rationally related and lead to frequency-locked oscillations. In the power spectrum of the pressure and intensity time series (Figs. 4-IVa(iii) & -IVb(iii)), we see frequencies that are rationally related to f_1, leading to a frequency-locked behavior [20]. In the phase portrait (Figs. 4-IVa(i) & -IVb(i)), we find the trajectory no longer wanders on a torus, but instead, closes onto itself and hence, a periodic loop is formed. The time period is very long so we see many loops in the phase portrait. This is further seen in the Poincaré section (Figs. 4-IVa(ii) & -IVb(ii)) which has distinct points where the loop intersects the dotted Poincaré plane. The time taken by the system to complete one full cycle, seen in the time series, is equivalent to the time duration between point *a* and the local maxima adjacent to, and following point *h* (Fig. 7). Images $a-h$ correspond to different phases of the signal within this time duration.

Although oscillations are periodic in nature, since the total time period (time required for phase space trajectories to come back to the initial point) is much longer than a limit cycle, it is difficult to come to the same conclusion by looking at the instantaneous flame images. The flame oscillations are stronger when compared to limit cycle and quasi-periodic oscillations although the pressure amplitude from the time traces is the same. In image f, for example, the flame leaves the tip of the burner whereas in image e, it is on the verge of extinction. Images a, b, c and e are all at local maxima in the pressure time series, but each one has a completely different shape. The most interesting of the images shown is image c, where different flames in the multiple injection burner assume different lengths. As the flame location is varied, the flame location with respect to acoustic modes of the duct gets changed. The effect can be seen in flame images and also in the pressure and intensity time traces since the interaction is coupled.

Quasi-periodic oscillations with subharmonic frequency content: Region V. Following this state, the next bifurcation at $x_f = 25.5$ *cm*, results in a quasi-periodic state where the strength of the frequency f_1 decreases and f_2 emerges as the dominating frequency along with a frequency $\frac{f_2}{2}$. This is region V in Fig. 3. The attractor for this case is similar to the one discussed for the quasi-periodic oscillations in region III, the difference being in the presence of a subharmonic. The dynamics is dominated mostly by quasi-periodicity, except for a small region (the bulge within region V, Fig. 3a), where the subharmonic content grows but subsides before the system eventually goes to a period-2 oscillation.

Period-2 oscillations: Region VI. The quasi-periodic region with f_2 and its subharmonic now changes to a periodic oscillation, with frequency components f_2 and $\frac{f_2}{2}$ (Figs. 4-VIa(iii) & -VIb(iii)). The presence of a sub-harmonic leads to double-looped attractor in the phase space (Figs. 4-VIa(i) & -VIb(i)); i.e. the trajectories need to loop twice before coming back to the initial point. Since the orbit is periodic, we get two distinct dots in the single-sided Poincaré section for the pressure time series (Figs. 4-VIa(ii)) and set of four dots (scattered due to the noise in signal) in the double-sided Poincaré section (Figs. 4-VIb(ii)), in the case of flame intensity time series measurement.

In the flame shape modulations (Fig. 8), it can be seen that because of the period-2 nature, image frames separated by the time period corresponding to f are different. The pairs of images, *a* & *c*, *b* & *d*, *e* & *f* and *g* & *h* are each acquired almost at the same phase, separated by a time interval $\frac{1}{f}$ and are different in their intensities due to the period-2 nature of oscillations.

As we vary the flame location gradually, the system moves from period-2 oscillation to a chaotic state via quasi-periodic states. The quasi-periodic route to chaotic oscillations has been observed in several nonlinear systems such as Taylor-Couette flow [21] and Rayleigh-Bénard convection [22].

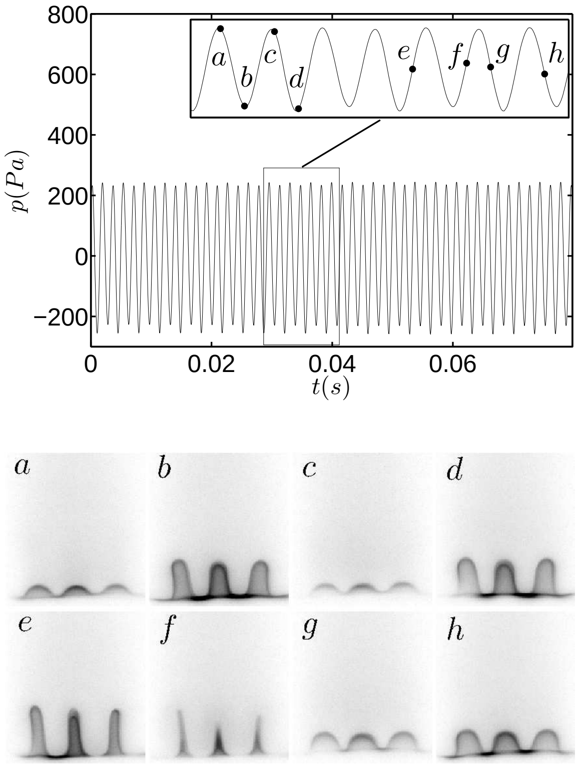

FIGURE 8: INSTANTANEOUS FLAME IMAGES FOR PERIOD-2 OSCILLATIONS. THE TAGGED DOTS IN THE PRESSURE TIME SERIES HAVE CORRESPONDING FLAME IMAGES MARKED BY THE SAME LOWERCASE ALPHABETS AS USED FOR THE TAGS.

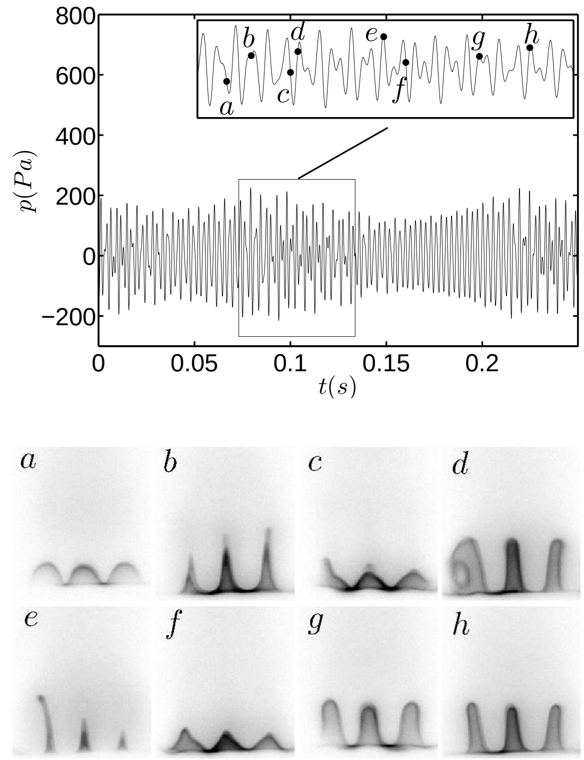

FIGURE 9: INSTANTANEOUS FLAME IMAGES FOR CHAOTIC OSCILLATIONS. THE TAGGED DOTS IN THE PRESSURE TIME SERIES HAVE CORRESPONDING FLAME IMAGES MARKED BY THE SAME LOWERCASE ALPHABETS AS USED FOR THE TAGS.

Chaotic oscillations: Region VII. At the onset of region VII, a strange attractor [14, 15] emerges in the system. An attractor is termed as strange when its calculated dimension is not an integer i.e. when the structure is a fractal. There are several measures to estimate the dimension of a set of points [16, 23]. The correlation dimension is one such measure. To calculate the correlation dimension, the correlation sum $C(r)$, given by Eq.1, is calculated for the attractor. We need not limit ourselves to a 3-dimensional phase space for calculating quantitative information.

$$C(r) = \lim_{r \to 0} \frac{1}{N^2} \left(\text{number of pairs of points with } E < r \right), \quad (1)$$

where, N is the number of points in the phase space and E is the euclidean distance between two points on the attractor. The correlation sum has a power law dependence on r as $r \to 0$ and the power on r gives the correlation dimension of the attractor [16]. The correlation dimension calculated for the attractor shown in Fig. 4-Va(i) observed in region (VII) is 2.63 - an indication that it is a strange attractor. To check if oscillations are chaotic, we need to calculate the maximal Lyapunov exponent. The maximal Lyapunov exponent is a measure of the exponential divergence or convergence of neighboring trajectories of an attractor. A chaotic attractor will have at least one positive Lyapunov exponent. On application of Kantz algorithm [24] for calculation of Lyapunov exponent for the chaotic attractor obtained here, we obtain a value of 0.16 which indicates that the attractor is chaotic. The route taken by our system to chaotic oscillations is a quasi-periodic route, similar to the Ruelle-Takens scenario in fluid dynamics [17]. As the flame location is changed, several incommensurate frequencies appear in the oscillations which eventually merge to form a broadband frequency spectrum as seen in Figs. 4-VIIa(iii) & -VIIb(iii). The intersection of this chaotic attractor with the Poincaré plane as shown in Figs. 4-VIIa(ii) & -VIIb(ii) leads to a set of points scattered on a plane due to the chaotic nature of oscillations.

Figure 9 gives the flame shapes at various phases as marked in the pressure time series data. The chaotic nature of oscillations is also reflected in the flame images. We find that the flame exhibits irregular modulations. Chaotic oscillations in the system are accompanied by rolling of the flame surface (image *d*), lifting-off (images *c* and *g*) and elongation (images *b* and *e*).

Following this chaotic state, the system jumps back to the stable state at $x_f = 48.5\ cm$. Going in the reverse direction (Fig. 3b) all the states discussed above appear again in exactly the reverse order but with a hysteresis in the flame location values where the different bifurcations occur.

DISCUSSIONS

In summary, we have shown in this paper that thermoacoustic oscillations exhibit a variety of nonlinear phenomena. A simple laboratory combustor running on lean premixed combustion is used to illustrate this point. For a constant equivalence ratio, the system goes from a steady state to limit cycle oscillations through a subcritical Hopf bifurcation, as flame location is varied. This is followed by a second Hopf bifurcation (Neimark-Sacker bifurcation) to a quasi-periodic state. On changing the flame location further, the quasi-periodic state becomes a periodic, frequency-locked state marked by several distinct peaks in the frequency spectrum at rationally related frequencies. Further, the system goes to another quasi-periodic state with subharmonic frequency content. This state exists for a long range of control parameter values and is followed by period-2 oscillations. The next bifurcation leads to a chaotic state through a quasi-periodic route, also known as the Ruelle-Takens scenario [17]. Eventually the system comes back to the steady state from the chaotic state directly. The complex nonlinear behavior of the system was reflected in the pressure time series, the flame intensity time series and simultaneously in the flame surface modulations in the instantaneous flame images. Nonlinear time series analysis made it possible to look at the oscillations through their phase space representation. This was instrumental in identifying the characteristics of oscillations and differentiating them from each other. A point to note further, is that due to the subcritical nature of the Hopf bifurcation, it is possible that, for different operating conditions, limit cycle oscillation is an unstable state. The self-excited oscillations at the Hopf point can be a period-2 oscillation generate d via secondary bifurcation. In fact, when the experiments were run for different equivalence ratios or flow rates, the self-excited oscillations obtained at the Hopf point were either period-2 or even quasi-periodic oscillations. A possible explanation for the rich nonlinear behavior is as follows. The phenomenon of combustion instability (in the system under study) is a result of interaction between the flame and the duct acoustic modes. Depending on the flame location, different acoustic modes are excited. As a result, the acoustic fluctuations at the flame location (combination of excited acoustic modes of the duct) varies as the flame location is changed. The nonlinear response of the flames to this acoustic field that is varying with the flame location could lead to the emergence of complex nonlinear oscillations. This complex nonlinear behavior; i.e., bifurcations and different oscillation states, is also be observed if other parameters such as the equivalence ratio or the mean flow rate are chosen as the control parameter.

Thermoacoustic instability, in general, induces high amplitude pressure oscillations within combustion systems. Looking at the results from a practical standpoint, the presence of nonlinear oscillations such as quasi-periodic, frequency-locked and chaotic oscillations, will cause further increase in thermal and mechanical loading to the combustor walls. Thus, leading to premature failure, accelerated crack growth, amplified wear and tear of structural components and higher fatigue loading. All these factors contribute to the reduction in the life span of combustors [25]. Furthermore, limit cycle oscillations consist of a single dominant frequency whereas, other classes of oscillations consist of a range of frequencies, which might include frequencies close to the natural frequency of some of the structural components of the system. As a result, thermoacoustic oscillations can cause resonance in structural components leading to violent vibrations in the system or even structural failure. A controller designed to handle a single frequency or a set of frequencies might fail in the presence of frequencies that have not been considered in the design process. From the results on high speed flame images, it is also seen that along with changes in the frequency content of pressure signals, the flame dynamics drastically changes, giving rise to extreme behavior such as lift-off and flame extinction. Such behavior is also unfavorable for real systems.

CONCLUSIONS

In this paper, we have seen that due to the nonlinear interactions between combustion and acoustics, a simple thermoacoustic system can exhibit a rich variety of dynamics. It is well known that the flame dynamics plays a crucial role in the phenomenon of thermoacoustic instability. Here, we further illustrate this point through flame images acquired for different classes of nonlinear oscillations. The observed oscillations were investigated in the light of nonlinear dynamics. We have reported a trend followed by our system with change in one of the system parameters. Changing other parameters or changing the same parameter for different conditions will give a different trend, however, the characteristics of the observed oscillations are expected to remain similar. Nonlinear time series analysis enables us to obtain an understanding of the system dynamics purely through experimental data. The information acquired could be critical in constructing accurate models for thermoacoustic systems and designing effective control strategies.

ACKNOWLEDGMENT

This work was funded by Department of Science and Technology, India.

NOMENCLATURE

I Flame intensity fluctuations.
$\mathscr{V}_a$ Volumetric air flow rate, *ccm*.
$\mathscr{V}_f$ Volumetric fuel flow rate, *ccm*.
f Frequency, *Hz*.
p Pressure fluctuations, *Pa*.
ϕ Equivalence ratio.
τ Time delay used for phase space reconstruction.
t Time, *s*.
x_f Flame location, *cm*.

REFERENCES

[1] Zinn, B. T., and Lieuwen, T. C., 2005. "Combustion instabilities: Basic concepts, chapter I, combustion instabilities in gas turbine engines: Operational experience, fundamental mechanisms, and modeling". *Progress in Astronautics and Aeronautics, AIAA, Inc*, ***210***, pp. 1–26.

[2] Lieuwen, T. C., 2002. "Experimental investigation of limit-cycle oscillations in an unstable gas turbine combustor". *Journal of Propulsion and Power*, ***18***(1), January, pp. 61–67.

[3] Schadow, K., and Gutmark, E., 1992. "Combustion instability related to vortex shedding in dump combustors and their passive control". *Progress in Energy and Combustion Science*, ***18***(2), pp. 117 – 132.

[4] Poinsot, T. J., Trouve, A. C., Veynante, D. P., Candel, S. M., and Esposito, E. J., 1987. "Vortex-driven acoustically coupled combustion instabilities". *Journal of Fluid Mechanics*, ***177***, pp. 265–292.

[5] Candel, S., 2002. "Combustion dynamics and control : progress and challenges". *Proceedings of the Combustion Institute, Pittsburgh, PA,*, ***29***, May, pp. 1–12.

[6] McManus, K., Poinsot, T., and Candel, S., 1993. "A review of active control of combustion instabilities". *Progress in Energy and Combustion Science*, ***19***(1), pp. 1 – 29.

[7] Moeck, J. P., Bothien, M. R., Schimek, S., Lacarelle, A., and Paschereit, C. O., 2008. "Subcritical thermoacoustic instabilities in a premixed combustor". *14th AIAA/CEAS Aeroacoustics Conference (29th AIAA Aeroacoustics Conference)*, May, pp. 1–18.

[8] Matveev, K. I., and Culick, F. E. C., 2003. "Limit-cycle properties of a Rijke tube". *Technical acoustics*, ***12***, pp. 1–13.

[9] Jahnke, C. C., and Culick, F. E. C., 1994. "An application of dynamical systems theory to nonlinear combustion instabilities". *Journal of Propulsion and Power*, ***10***(4), July-August, pp. 508–517.

[10] Sterling, J. D., 1993. "Nonlinear analysis and modelling of combustion instabilities in a laboratory combustor". *Combustion Science and Technology*, ***89***(4), March, pp. 167 – 179.

[11] Lei, S., and Turan, A., 2009. "Nonlinear/chaotic behaviour in thermo-acoustic instability". *Combustion Theory and Modelling*, ***13***(3), pp. 541–557.

[12] Matsui, Y., 1981. "An experimental study on pyro-acoustic amplification of premixed laminar flames". *Combustion and Flame*, ***43***, June, pp. 199–209.

[13] Noiray, N., Durox, D., Schuller, T., and Candel, S., 2008. "A unified framework for nonlinear combustion instability analysis based on the flame describing function". *Journal of Fluid Mechanics*, ***615***, July, pp. 139–167.

[14] Nayfeh, A. H., and Balachandran, B., 2004. *Applied Nonlinear Dynamics: Analytical, Computational, and Experimental Methods*. Wiley-VCH Verlag GmbH & Co. KGaA, Weinheim.

[15] Strogatz, S. H., 2007. *Nonlinear Dynamics And Chaos: With Applications To Physics, Biology, Chemistry, And Engineering*. Levant Books.

[16] Moon, F. C., 2004. *Nonlinear Chaotic and Fractal Dynamics: An Introduction for Applied Scientists and Engineers*. Wiley-VCH Verlag GmbH & Co. KGaA, Weinheim.

[17] Ruelle, D., and Takens, F., 1970. "On the nature of turbulence". *Communication in Mathematical Physics*, ***20***, October, pp. 167–192.

[18] Abarbanel, H. D. I., 1996. *Analysis of Observed Chaotic Data*. Springer-Verlag New York, Inc.

[19] Kantz, H., and Schreiber, T., 2003. *Nonlinear Time Series Analysis*. Cambridge Press.

[20] Hilborn, R. C., 2000. *Chaos and Nonlinear Dynamics: An Introduction for Scientists and Engineers*. Oxford University Press.

[21] Brandstater, A., Swift, J., Swinney, H. L., Wolf, A., Farmer, J. D., Jen, E., and Crutchfield, P. J., 1983. "Low-dimensional chaos in a hydrodynamic system". *Phys. Rev. Lett.*, ***51***(16), October, pp. 1442–1445.

[22] Gollub, J. P., and Benson, S. V., 1980. "Many routes to turbulent convection". *Journal of Fluid Mechanics.*, ***100***, September, pp. 449–470.

[23] Grassberger, P., and Procaccia, I., 1983. "Characterization of strange attractors". *Physical Review Letter*, ***50***(5), January, pp. 346–349.

[24] Kantz, H., 1994. "A robust method to estimate the maximal Lyapunov exponent of a time series". *Physics Letters A*, ***185***, January, pp. 77–87.

[25] Suresh, S., 1998. *Fatigue of Materials*. Cambridge University Press.